Kilometric wave emission observed on pre-midnight side in the vicinity of the Earth's magnetic equatorial plane at 1-2 L-Shell

M.Y. Boudjada[1], P.H.M. Galopeau[2], S. Sawas[3], V. Denisenko[4,5], K. Schwingenschuh[1], H. Lammer[1], H.U. Eichelberger[1], W. Magnes[1], and B. Besser[1]

[1]Space Research Institute, Austrian Academy of Sciences, Graz, Austria
[2]LATMOS-CNRS, Université Versailles Saint-Quentin-en-Yvelines, Guyancourt, France
[3]Institute of Communications and Wave Propagation, University of Technology, Graz, Austria
[4]Institute of Computational Modelling, Russian Academy of Sciences, Krasnoyarsk, Russia
[5]Siberian Federal University, Krasnoyarsk, Russia

Correspondence: M.Y. Boudjada (mohammed.boudjada@oeaw.ac.at)

Abstract. The ICE experiment onboard the DEMETER satellite recorded kilometric wave emissions in the vicinity of the magnetic equatorial plane. Those radiations were observed in the beginning of the year 2010 on the night-side of the Earth and rarely on the day-side. We distinguish two components one appears as a continuum between few kHz and up to 50 kHz and the other one from 50 kHz to 800 kHz. The first component exhibits positive and negative frequency drift rates in the southern and northern hemispheres, at latitudes between 40° and 20°. The second component displays multiple spaced frequency bands. Such bands mainly occur near the magnetic equatorial plane with a particular enhancement of the power level when the satellite latitude is close to the magnetic equatorial plane. We show in this study the similarities and the discrepancies between DEMETER kilometric emission and the well-know terrestrial kilometric radiation. We believe that both emissions are the signatures of the radio sources localized in the inner and outer parts of the plasmasphere. The hollow cones of the DEMETER kilometric wave emissions are oriented towards the Earth's ionosphere, and not the magnetosphere. We suggest that such emissions are associated to Z-mode trapped region only detectable by electric field experiment onboard low Earth orbiting satellite at altitudes less than 700 km.

1 Introduction

A variety of radio waves have been detected in the near Earth's space environment in the seventies. Imp 6 satellite radio measurements have allowed the identification, for a first time, of a weak continuum associated to the Earth's magnetosphere. The continuum power level was found to be below the cosmic noise level at frequencies of about 100 kHz with a low frequency of 30 kHz (Brown, 1973) which was considered to be produced by solar wind local plasma frequency. Another continuum component but more intense have been identified at even lower frequencies, between 5 and 20 kHz (Gurnett and Shaw, 1973). This radiation is found to occur at frequencies smaller than the local plasma frequency of the solar wind. Gurnett (1975) showed that these two types of emission belong to a single non-thermal continuum spectrum, one 'trapped' and the other 'escaping'. The first component has frequencies lower than about 30 kHz which correspond to the magnetopause plasma frequency, and the second one has frequencies above this limit. Kurth et al. (1981) showed using ISEE 1 satellite quite temporal and spectral differences between both components. The observed differences are interpreted as the effect of the cavity on the 'trapped' component. Also high resolution spectrograms made evident the presence of numerous narrow-band emissions for the 'escaping' component.

Recent missions like CLUSTER, GEOTAIL, IMAGE and INTERBALL-1 provide new observations of the terrestrial nonthermal continuum. Hashimoto et al. (1999, 2006) reported about a new component at frequencies of 100 to 800 kHz detected when GEOTAIL satellite was at 10 to

30 R_E inside the Earth's magnetosphere. About one hundred events were recorded during the period from 01st Jan. to 31st Dec. 1996. Events were found to occur on the dayside/evening sectors and within about $10°$ of the magnetic equator. Kuril'chik et al. (2001, 2007) reported events of kilometric continuum recorded by INTERBALL-1 satellite very close to the Earth (1.6 to 2.4 R_E) with a high spectral resolution (10 kHz and 0.2 sec) at two frequencies 252 kHz and 500 kHz. Authors showed that the 'continuum' emission has a rather impulsive character, and a dependence of the beam widths on the solar activity. The polar orbit of the IMAGE satellite allowed finding that the nonthermal continuum radiation extends from about 29 kHz to about 500 kHz and forming a 'Christmas tree' pattern, nearly symmetric about the magnetic equator (Green and Boardsen, 2006). IMAGE satellite observations showed that the kilometric continuum is confined to a narrow latitude range of about $15°$. The source region of the kilometric continuum is found in the plasmapause within notch structures co-rotating with the Earth (Green et al., 2004). First CLUSTER non-thermal continuum observations were reported by Décréau et al. (2001). Direction finding technique, based on antenna spin modulation, allowed localizing the source regions in the plasmapause (Décréau et al., 2004) confirming IMAGE observations. CLUSTER tetrahedral configuration of four identical satellites allowed the analysis of specific type of nonthermal continuum. Hence Grimald et al. (2008) showed in the nonthermal emissions the presence of spectral peaks organized as several banded emissions with a frequency interval nearby the gyrofrequency at the source. Also details on the wave spectral signature was investigated by El–Lemdani Mazouz et al. (2009) particularly the splitting in fine frequency bands. Another type called 'nonthermal continuum patches' were found to occur within a relatively short time and over a wide frequency range (Grimald et al., 2011). Authors showed that 'patches' events represent 25% of the total nonthermal emissions recorded in one year.

Physical mechanisms at the origin of the terrestrial nonthermal continuum were first proposed by Frankel (1973) who considered gyro-synchrotron radiation linked to energetic electrons. Gurnett and Frank (1976) made evident correlation between continuum radiation and 1 to 30 keV electrons. Such electrons injection let to intense electrostatic waves nearby the upper hybrid resonance frequency. A linear conversion model was suggested by Jones (1976, 1977) where electrostatic waves in the presence of a density gradient would convert into ordinary mode radio waves. In the source region, the density gradient must be nearly perpendicular to the magnetic field. This model predicts a beamed radiation outward in two meridionals beams at angles of $\gamma = \pm arctan(fc/fp)^{1/2}$ with regard to the magnetic equator. Those angles are depending on f_p the electron plasma frequency and f_c the cyclotron frequency. Also Jones model expects that the generated O-mode emission should be left-hand polarized. The beamed radiation and the O-mode po-

larization have been confirmed, respectively, by Jones et al. (1987) and Gurnett et al. (1988).

In this paper, we analyze the kilometric wave radiation observed by ICE/DEMETER experiment in the beginning of the year 2010. The characteristics of this radiation, essentially the spectral features and the spatial occurrence are described in Section 2. Discussion of the outcomes is detailed in Section 3 where principally our results are combined to previous ones. Summary of the main results are given in Section 4.

2 Kilometric radio emission

2.1 Overview of HF/ICE observations

We consider in this study the space observations provided by the DEMETER microsatellite. The aim is the analysis of particular spectral features recorded by the ICE experiment in the beginning of the year 2010, i.e. January, February and March. The ICE instrument allows a continuous survey of the electric field over a wide frequency range, from few Hz up to about 3.5 MHz (Berthelier et al., 2006). The electric field component is determined along the axis defined by two sensors. The satellite sun-synchronous half-orbit duration is about 40 min and covering invariant latitude between -65° and +65°. The DEMETER satellite orbits are associated to two fixed local times (LTs), at about 10 LT and 22 LT. We use in this investigation the survey mode of the ICE experiment covering the frequency range between few kHz and 3.5 MHz, called hereafter HF-band. The radio wave emissions are alternately recorded on the day- and night-sides of the Earth corresponding respectively to down and up half-orbits. However the main radiations investigated in this paper are observed on the night-side, and rarely on the dayside. Generally the ICE HF-band dynamic spectra allow distinguishing three kinds of spectral emissions depending on the satellite geographical latitudes. The first one is recorded close to the sub-auroral regions at latitudes between 50° and 60°; it mainly concerns the auroral kilometric radiation described by Parrot and Berthelier (2012). The second are mainly ground-based transmitters, low frequency (LF) radiation, appearing at mid-latitudes between 50° and 20°, in both hemispheres (e.g., Parrot et al., 2009; Boudjada et al., 2017).

The third kind of emission is a kilometric wave radiation occurring in the vicinity of the equatorial magnetic plane at low latitudes. Hereafter we focus on the analysis of the kilometric radiation in particular the spectral characteristics, the magnetic latitude and the power intensity occurrence. Also the dependence of the power level on the frequency and the magnetic latitude is considered. We use a manually technique which consists to follow and to save with the PC-computer mouse the frequency and the temporal evolution of the radiation. The saved parameters are the observation time (UT hours), the frequency (kHz) and the power level

$(\mu V m^{-1} H z^{-1/2})$. The collected points are later combined with the satellite orbital parameters like the magnetic latitude and the L-Shell.
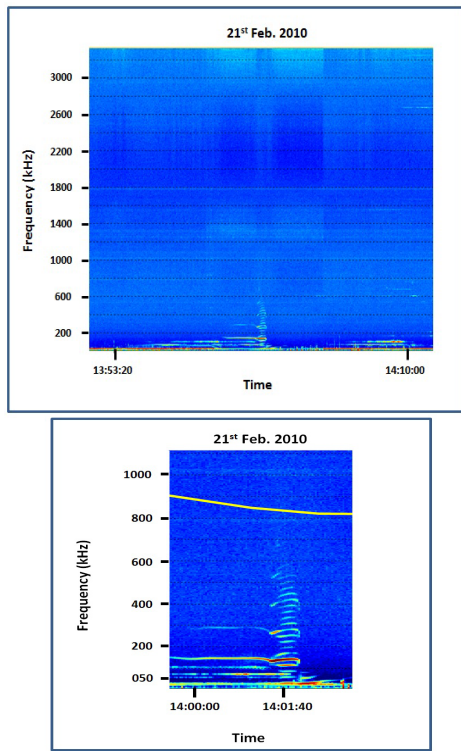
Figure 1. Example of kilometric wave emission recorded by the ICE/DEMETER on 21st Feb. 2010. The first panel displays an overview of the dynamic spectrum in the frequency range from few kHz to 3.5 MHz. The second panel shows a zoomed part for the event in the frequency bandwidth between few kHz and 1100 kHz. The gyro-frequency is indicated by the yellow curve.

2.2 Frequency and time characteristics

The DEMETER ICE experiment detected kilometric wave emissions in the frequency range between few kilohertz and up to 800 kHz. Two examples recorded on the night-side are shown in Fig.1 and Fig.2. First panel of Fig.1 displays the dynamic spectrum recorded by ICE experiment on 21st Feb. 2010 between 13:52 UT and 14:12 UT. The satellite was on the late evening sector, around 22 LT, at a distance of 665 km. In this time interval the satellite geographical coordinate varied from -18°S to +04°N in latitude and 142° to 138° in longitude. The second event shown in the first panel of Fig.2 was also recorded at about 22 LT at similar distance from the Earth. Satellite geographical coordinate varied from -25°S to 40°N in latitude and 117° to 102° in longitude in the time interval between 14:10 UT and 14:26 UT. Second panel of Fig.1/Fig.2 displays a zoomed part of the dynamic spectrum shown in the first panel where the kilometric wave emission

appears in the frequency range between few kHz and up to 800 kHz. One note on both second panels of Fig.1 and Fig.2, changes in the spectral kilometric wave emissions before and after 50 kHz. Hence the first radiation appears as a narrow continuum with an instantaneous bandwidth of about 2 kHz at frequencies less than 50 kHz. It displays negative and positive frequency drifts when the satellite is approaching or leaving the equatorial plane, respectively. Its frequency drift rate is weak and in the order of 0.2 kHz/s. The second emission is composed of parallel narrow-bands in a frequency above 50 kHz and up to 800 kHz. The band time duration is, on average, of about 1 minute and decreases to less than one minute when the emission frequency increases. The frequency bandwidth varies from few kHz and up to 20 kHz. Some narrow-bands showed a high power level (red color in Fig.1/Fig.2) when they are compared to other narrow bands. Those enhanced emission bands exhibit an extensive time duration of about 3 minutes.
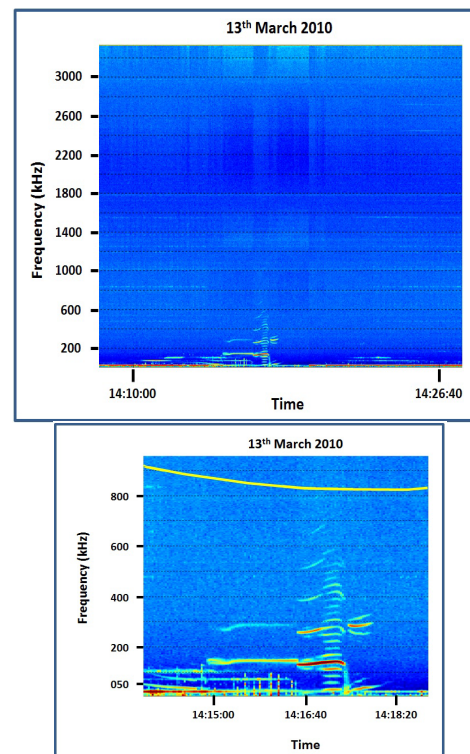
Figure 2. Like in Fig.1 for an event recorded by DEMETER on 13th March 2010.

2.3 Magnetic latitude and power level occurrence

The kilometric wave radiation occurrences in magnetic latitude and power level are shown, respectively, in the top and the bottom panels of Fig.3. The main kilometric emission were recorded when DEMETER was in the southern part of the magnetic equatorial plane. Hence the emissions are de-

tected in the magnetic latitude range between -40° and 20°, as shown in the first panel of Fig.3. We note a clear progressive increase of the kilometric emission occurrence which reaches a maximum at magnetic latitude of -10°. More than
5 90% of the kilometric radiation occurred in magnetic latitude range between -50° and 0°. Sudden decrease of the occurrence is recorded when the satellite crosses the magnetic equatorial plane. Emission is found to be more extended in the southern hemisphere with a clear di–symmetry occur-
10 rence before and after the equatorial magnetic plane.
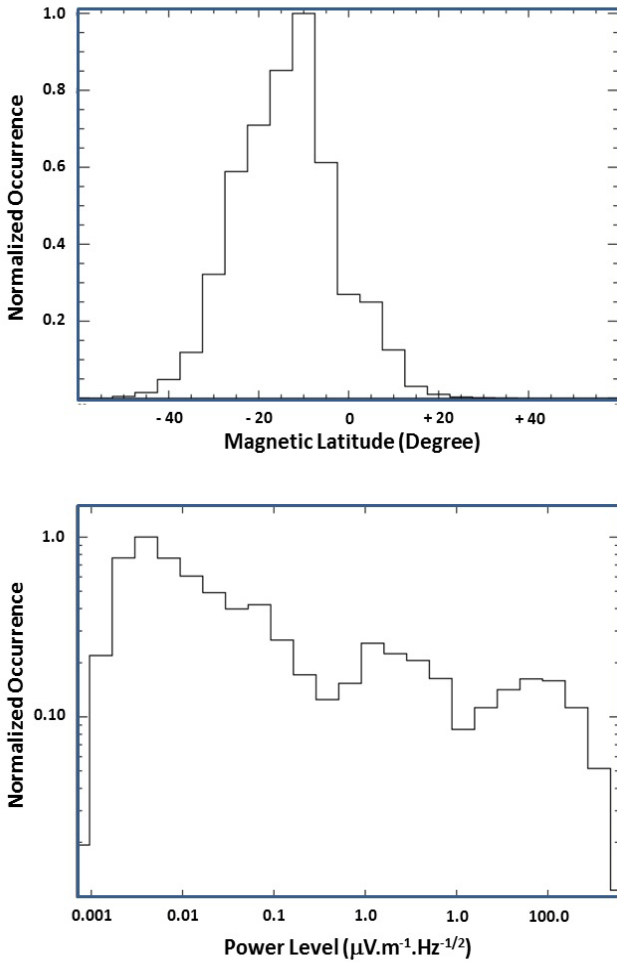
Figure 3. Occurrence of kilometric wave emissions in magnetic latitude (Degree) and in power level ($\mu V m^{-1} H z^{-1/2}$).

The power level, as displayed in the second panel of Fig.3, is covering a large interval between 10^{-3} $\mu V m^{-1} H z^{-1/2}$ and 10^{+4} $\mu V m^{-1} H z^{-1/2}$. More than 70% of emissions have a level less than 1 $\mu V m^{-1} H z^{-1/2}$ and belong mainly
15 to the southern hemisphere. Above this weak power level, the occurrence of the kilometric emission is associated to both hemispheres. The intense power level is associated to the kilometric emission occurring mainly at lower frequency,

i.e. from few kilohertz and up to 100 kHz. We distinguish three occurrence maxima at about 5x 10^{-3} $\mu V m^{-1} H z^{-1/2}$, 20
1 $\mu V m^{-1} H z^{-1/2}$ and 80 $\mu V m^{-1} H z^{-1/2}$. We separate the power level by taking into consideration the interval associated to the previous maxima. Hereafter green, blue and red colors indicate, respectively, three power level intervals, i.e.
0.001 - 0.7 $\mu V m^{-1} H z^{-1/2}$, 0.7 - 10 $\mu V m^{-1} H z^{-1/2}$, and 25
10 - $\mu V m^{-1} H z^{-1/2}$.
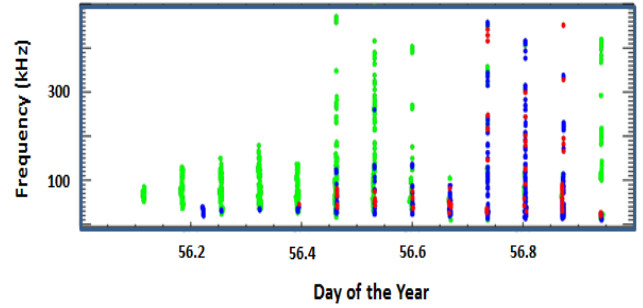
Figure 4. Vertical lines indicate the occurrence of the kilometric emissions observed on 25th Feb. 2010. Those events were recorded on the night-side of the Earth with a time interval of about 01h35mnin. Green, blue and red colors specify, respectively, three power level intervals, i.e. $10^{-3} - 0.7$ $\mu V m^{-1} H z^{-1/2}$, 0.7 - 10 $\mu V m^{-1} H z^{-1/2}$, and $10 - 10^{+4}$ $\mu V m^{-1} H z^{-1/2}$.

Kilometric wave emissions are regularly observed on the nigh-side (22 LT) before and after the magnetic equatorial plane in the vicinity of the Earth at a distance less than 750 km. Fig.4 displays the daily occurrence of kilometric emis- 30 sions on 25th Feb. 2010. We observe a periodic occurrence of the emission with a time interval of about 1h35 which corresponds to a DEMETER microsatellite full orbit. Each vertical line is considered as an 'event' and corresponds to the recorded emission for a given half-orbit. The occurrence per 35 day is about 13 events in the optimal case. However from one event to another we find a variation in the frequency bandwidth and also in the power level.

2.4 Power level versus frequency and magnetic latitude

Fig.5 displays the power level variation versus the magnetic 40 latitude where the colors indicate different power levels as defined in the previous sub-Section. The weakest intensities (less than 0.7 $\mu V m^{-1} H z^{-1/2}$) are recorded at magnetic latitudes between -50° and +30° but much more in the southern hemisphere, as displayed in first panel of Fig.5. Structured 45 emissions appear when the magnetic latitude is positive principally after the crossing of the magnetic equatorial plane. One can distinguish five components appearing in four frequency ranges: few kHz - 50 kHz, 70 kHz - 130 kHz, 170 kHz - 250 kHz, 280 kHz -340 kHz and 380 kHz- 420 kHz. 50 Those radiations are extended in magnetic latitudes in par-
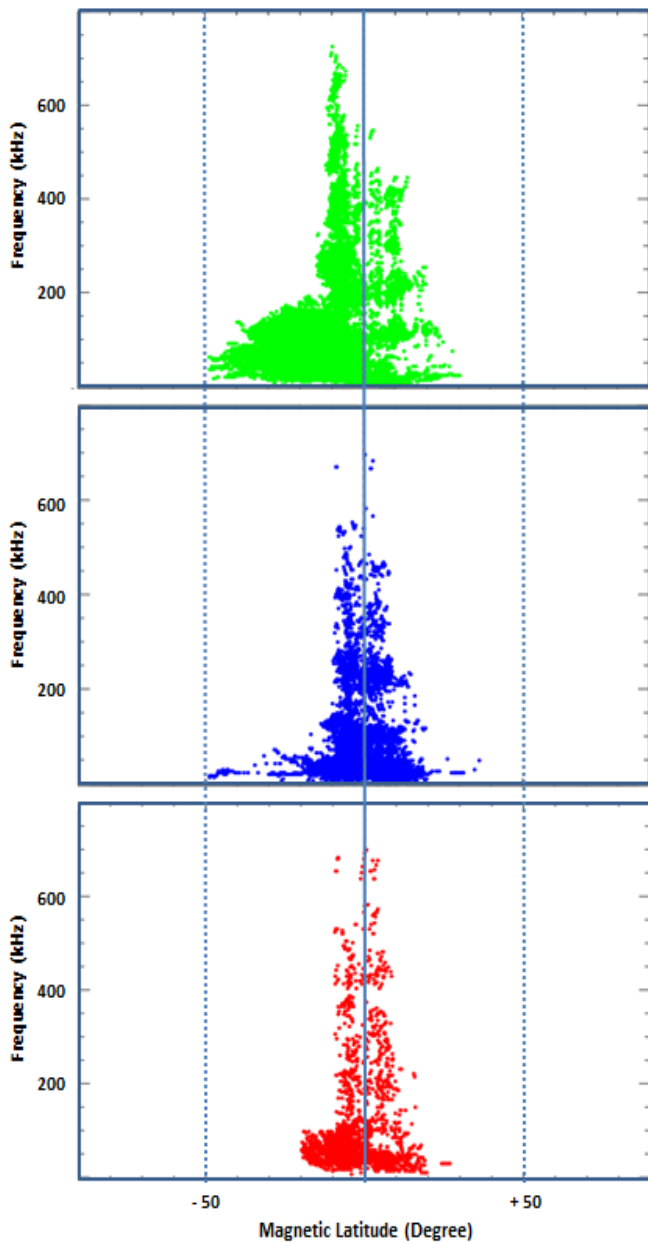
Figure 5. Variation of the power levels versus the frequency (vertical axis) and the magnetic latitude (horizontal axis) for all events. Colors are similar to those used in Fig.4. Green, blue and red colors specify, respectively, three power level intervals, i.e. $10^{-3} - 0.7 \ \mu V m^{-1} H z^{-1/2}$, 0.7 - 10 $\mu V m^{-1} H z^{-1/2}$, and $10 - 10^{+4}$ $\mu V m^{-1} H z^{-1/2}$.

ticular at low frequencies around 50 kHz, and decreases at higher frequencies, at about 400 kHz. Kilometric wave emission is quasi-absent between those four frequency bands.

Also structured emissions are observed in the southern part of the magnetic equatorial plane at frequencies above 200

kHz in magnetic latitude between -10° and 0° degrees, as shown in the first panel of Fig.5. Those structures are mainly extended in frequency, contrary to those observed in northern hemisphere which extended in magnetic latitude. We distinguish four components occurring in the following frequency bands: 200 kHz - 320 kHz, 320 kHz - 450 kHz, 450 kHz - 570 kHz and 570 kHz - 670 kHz. At frequencies lower than 200 kHz, we note a quasi-absent of structured emission in the southern hemisphere. Kilometric radiations continuously occur in magnetic latitude between -50° and 0°. In this interval, we find a positive/negative frequency drift rate of about +3.75 / -1. 25 kHz/degree when the frequency is higher/smaller than 50 kHz. The kilometric emissions is mainly confined to frequencies lower than 150/100 kHz in the southern/northern part of the magnetic equatorial plane when the power level is between 0.7 and 10 $\mu V m^{-1} H z^{-1/2}$, as displayed in the second panel of Fig.5. Above 150 kHz, the radiations only occur in the frequency bandwidth 180 kHz to about 250 kHz. The power level in the range 10 - 10^4 $\mu V m^{-1} H z^{-1/2}$ is shown in the third panel of Fig.5. The main emission is nearly symmetrical distributed around the magnetic equatorial plane, between -10° and +10°, predominantly above 100 kHz. Below this limit, the radiation covers larger magnitude latitude from -20° to about +20°.
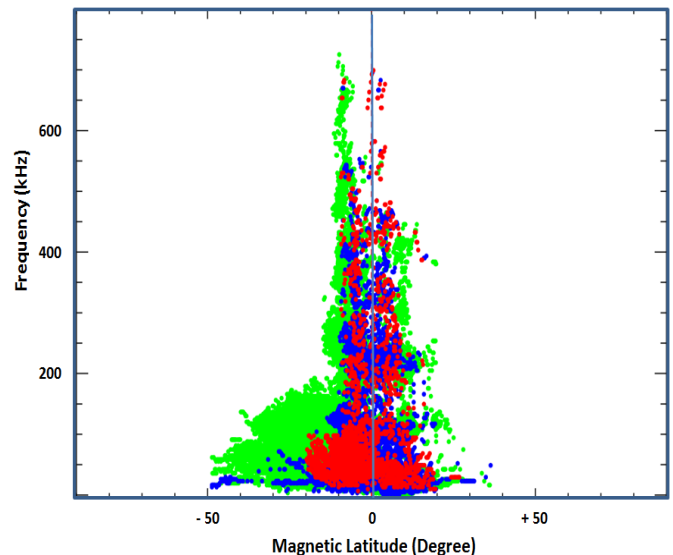
Figure 6. Overlapping of the three power levels displayed in Fig.5. The spectral pattern looks like a 'Christmas tree' with a 'trunk' along the magnetic equatorial plane.

The overlapping of the three power levels, as shown in Fig.6, allow getting a global shape similar to a 'Christmas-tree' pattern. We see globally that the kilometric emission is extensively occurring at frequency lower than 150 kHz, and starts to be less confined to the magnetic equatorial plane above this frequency limit. A cut-off appears around 50 kHz

which decrease to about few kHz when approaching the magnetic equator plane. This cut-off is characterized by a small frequency drift rate in latitude and a power level in the interval 0.7 and 10 $\mu V m^{-1} H z^{-1/2}$, i.e. blue color boundary in Fig.6. A second cut-off can be seen when the DEMETER satellite was in the southern hemisphere and absent in northern hemisphere. It starts at latitudes of about -40° and disappears at -18° when the frequency decreases from 150 kHz to 50 kHz. We find that both cut-offs intersected at frequency of about 50 kHz when the magnitude latitude is about -18°.

3 Discussion

We discuss hereafter the kilometric wave emission as detected by the DEMETER microsatellite. First we emphasis on the beaming of such emissions and how it extended and restrained around the magnetic equatorial plane. Then the similarity and the discrepancy between DEMETER kilometric emission and the terrestrial kilometric radiations are addressed. This is followed by a discussion on the generation mode and the source location.
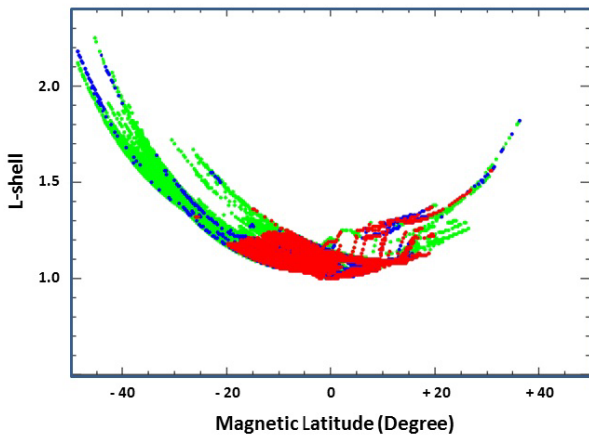
Figure 7. Variation of the kilometric wave emission versus the L-Shell and the magnetic latitude.

3.1 Beaming of the kilometric wave emission

The passage of DEMETER satellite through the magnetic equator lead to characterize a kilometric radiation recorded in the vicinity of the magnetic equatorial plane. The capability of DEMETER satellite leads to regularly recorded such type of emission at low altitudes around 700 km. We have found that the kilometric radiations exhibit different spectral patterns when the frequency is smaller or bigger than 50 kHz. The satellite recorded emissions on both side of the magnetic equator, and they appear to be more structured bands in the northern hemisphere. Those lasting bands indicate a 'stable' features in the late evening sector at about 22 LT.

The power level distribution of the kilometric emission shows restrained and extended deployment around the equatorial magnetic plane. Hence the latitudinal beam is found to be of about 40° when the frequency is, on average, less than 100 kHz. Above this limit and up to about 800 kHz, the latitudinal beam is decreasing and found of about 20°. This general picture is easily seen in the third panel of Fig.5. However we note a clear difference in the beam when the level is less than 1 $\mu V m^{-1} H z^{-1/2}$, as showed in the first panel of Fig.5. Hence the kilometric wave radiation beam is different when combing the emission recorded in the southern and northern parts of the magnetic equatorial plane. In the southern one, half of the spectral pattern is observed, i.e. beams of 25° and 10°, on average, in the frequency bandwidths 30 kHz-100 kHz and 100 kHz-800 kHz, respectively. On the other side of the equatorial magnetic plane only branches, or limbs, are detected as shown in the first panel of Fig.5. It is evident that emission diagrams are unlike which may be due to combine effects of multi-sources locations and ray path propagations.

The beams of the kilometric events are found to depend on the satellite orbits with regard to the magnetic equatorial plane. The two beams associated to the southern hemisphere events are observed in different frequency bandwidth. We may be deal with two source regions localized in the southern part of the magnetic equator but confined to two unlike regions with high and low plasma densities. Fig.7 displays the variation of the L-shell associated to the kilometric events versus magnetic latitude of the satellite. The power level is principally found to increase between 1 and 1.4 L-shell when the magnetic latitude of DEMETER is in between -20° and +20°. The source locations of kilometric wave radiation seem to be confined to a narrow L-shell region.

Fig.8 provides a sketch of the emission diagrams of the kilometric wave emissions. Those diagrams are different before and after the magnetic equatorial plane. Hollow cones may be considered in the 'southern' source emission with opening angle which is small at frequency of about 700 kHz and increase to 40° around 100 kHz. Multi-beams can be related to the 'northern' sources which looks like a succession of 'laser-beams' emitting at specific frequencies.

3.2 Similarity and discrepancy with the terrestrial kilometric emission

Kilometric wave emission features, as investigated in this paper, allow us to address questions concerning its origin. We have found some spectral patterns which are similar to those reported in the literature in the case of the terrestrial kilometric emissions.

First, we have described changes of the spectral kilometric emissions at frequencies of about 50 kHz. Such frequencies boundaries are similar to those observed by other satellite observations, like Cluster, GEOTAIL and IMAGE. Hence the terrestrial kilometric radiation is trapped and escaping when the frequency is, respectively, smaller and bigger than
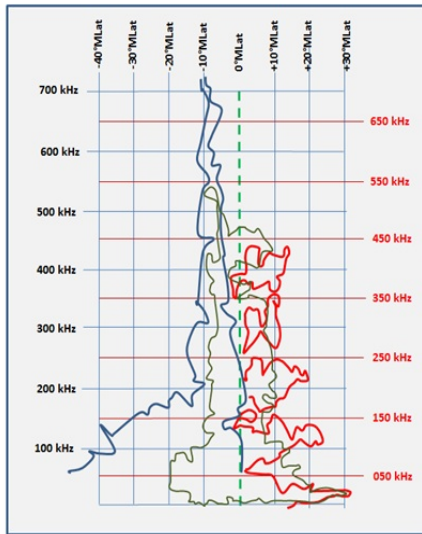
Figure 8. Sketch of the beams observed in the southern (blue color) and the northern (red color) parts of the magnetic equator plane, as resulting from Fig4b. The strong power levels (green-dark color) are recorded at $\pm 10°$ magnetic latitude.

50 kHz. The spectral features are often comparable and the main alternations may be due to the instrumental time and frequency resolutions, and also the satellite orbits with regard to the source locations. For example, the parallel narrow bands as displayed in Fig.5 are mainly associated to the escaping continuum in the case of the terrestrial kilometric emission. Hence Green and Boardsen (2006) show a typical sample of the kilometric continuum recorded by RPI/IMAGE experiment during a passage of the magnetic equator plane. AKR-X/INTERBALL-1 experiment provided similar emissions particularly in the southern hemisphere at low magnetic latitude and at L-Shell of about 1.2 (Kuril'chik et al., 2001). Observations at fixed frequencies (100 kHz, 252 kHz, 500 kHz and 749 kHz) allowed the analysis of the spectral character of such emissions. Authors showed that the terrestrial kilometric radiation occurrence is depending on the solar activity. Such radiation is regularly recorded during quiet solar activity. Our observations were registered in the begging of the year 2010, nearly eighteen months after the minimum of solar activity, i.e. Aug. 2008. Also the spectral pattern looks like a 'Christmas-tree' as also reported by Green and Boardsen (2006) in their review about the kilometric continuum radiation and it is confined to the magnetic equatorial plane.

Despite those common spectral features, several other observational aspects are different when combining the terrestrial kilometric radiation and the kilometric wave emission. The investigated DEMETER emission is detected at distance of about $1.1R_E$ which is generally not the case of the terrestrial kilometric emission. For instance GEO-TAIL and CLUSTER observations recorded radiation at more than $15R_E$ as reported by Hashimoto et al. (1999) and (Décréau et al., 2004), respectively. Also, the trapped or the escaping component is linked to terrestrial kilometric radiation recorded,respectively, between the plasmasphere and the magnetosphere, or outside of the magnetosphere. This radiation propagate largely in the free space in the L-O mode above the local plasma frequency linked to sources at or very near the plasmapause (Hashimoto et al., 2006). Also the gyro-frequency is found to be smaller than the trapped and the escaping frequencies as recorded by RPI/IMAGE experiment (see Fig.2 of Green and Boardsen (2006)). All those observational parameters are not similar to those reported in the case of the kilometric wave emission recorded by DEME-TER satellite.

3.3 Micro-scale features of the inner part of the plasmasphere

It is clear that both radiations have common spectral features but several discrepancy observational aspects linked to the generation mechanism. However the source locations should be the plasmasphere. Hence the terrestrial kilometric radiation is linked to plasmaspheric sources with emission beams oriented towards the magnetosphere. However the beaming of the DEMETER kilometric wave emissions is towards the Earth's ionosphere with sources localized in the plasmasphere. It is important to note that the DEMETER kilometric events belongs to a very limited regions in range 1-2 L-Shell (as shown in Fig.7) with distances between $1.1040R_E$ and $1.1070R_E$. This means that the DEMETER orbits is crossing the plasmaspheric hollow cones on few dozen of kilometer. Probably such restricted regions may be associated to the Z-mode waves which are linked to the free escaping L-O mode as suggested by Jones (1976) in his model. In such region the Z-mode waves are considered to be trapped and later converted into L-O mode associated to the terrestrial kilometric radiation. Green and Boardsen (2006) investigated and reported about the linear mode conversion theory based on Jones model. Authors showed profiles of plasmaspheric plasma frequency taking into consideration the Z-mode and the equatorial gyro-frequency. Regions of sharp plasma gradient are found and shown in Fig.5 of their paper. Carpenter et al. (2003) found similar region where ray paths of Z-mode echoes from radio sounding were recorded by IMAGE satellite in the polar regions.

We estimate the relationship between the Z-mode frequency (f_z), the plasma frequency (f_p) and the gyro-frequency (f_g) using the following formulae: $f_z = (f_g/2)[-1 + (1 + 4(f_p/f_g)^2)^{1/2}]$ (Carpenter et al., 2003). Fig.9 displays the variation of the three frequencies (i.e. f_z, f_p and f_g) versus the geocentric distance. The trapping region is localized between the lower and the higher f_z (green color in Fig.9) mainly between 1 kHz and 100
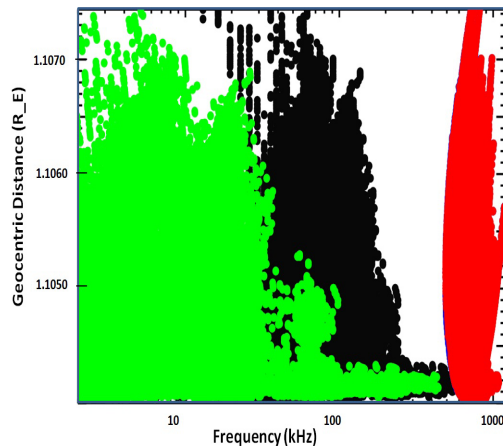
Figure 9. Variations of the kilometric wave emission versus the geocentric distance expressed in R_E. The green, black and red colors are associated, respectively, to f_z, f_p and f_g frequencies.

kHz, and extended up to 700 kHz. The plasma frequency is following the trapping region and starting at about 10 kHz and up to 800 kHz. The gyro-frequency appears at higher frequencies, i.e. above 800 kHz. Those features are com-

5 parable to previous investigations, e.g. Gurnett and Shaw (1983) and Carpenter et al. (2003) but in other regions.

4 Conclusion

We have investigated the kilometric wave radiation recorded by ICE/DEMETER experiment. DEMETER orbits allow us

10 to regularly record the kilometric radiation where, in the optimal case, about 13 events are daily registered. The power level is found in the interval between 10^{-3} $\mu V m^{-1} H z^{-1/2}$ and 10^{+4} $\mu V m^{-1} H z^{-1/2}$. The spectral analysis leads to find a 'Christmas-tree' which is the traces of the beaming

15 of the kilometric wave radiation. We have shown that those beams are not similar and depend on the emission frequency and the magnetic latitude. DEMETER kilometric emission can be comparable to the well-know terrestrial kilometric radiation. However several other observational aspects are

20 different when combining both emissions in particular the generation modes. We suggest that the DEMETER kilometric emissions are linked to a Z-mode micro-scale region. This trapping Z-mode region can only be detected between the Earth's ionosphere and the plasmasphere. The hollow

25 cones of this kilometric wave emissions are crossed by the DEMETER orbits at altitudes lower than 700 km. Probably the source regions of the DEMETER kilometric emission should be the plasmasphere, like the terrestrial kilometric radiation. IMAGE investigations reported about den-

30 sity structures recorded by EUV experiment (Burch et al., 2000) where new terms have been defined like channels and

crenulations (Darrouzet et al., 2009), and also a time evolution of the plasmasphere in particular on the pre-midnight sector (Sandel et al., 2003). We may consider that DEME-

35 TER orbits allow to investigate the inner part of the plasmasphere when other missions (i.e. GEOTAIL, IMAGE, INTERBALL) lead to study the outer part of the plasmasphere.

Acknowledgements. Acknowledgements. We acknowledge C. N. E. S. for the use of the DEMETER data, and thankful to Jean-Jacques Berthelier who provided us with data from the electric field experi-

40 ment (Instrument Champ Électrique – ICE).

References

Berthelier, J.J., Godefroy, M., Leblanc, F., Malingre, M., Menvielle, M., Lagoutte, D., Brochot, J.Y., Colin, F., Elie, F., Legendre, C., Zamora, P., Benoist, D., Chapuis, Y., Artru, J., and R. Pfaff, ICE,

45 the electric field experiment on DEMETER, Planet. Space Sci., 54, 456–471, 2006.

Boudjada, M.Y., P.F. Biagi, E. Al-Haddad, P.H.M. Galopeau, B. Besser, D. Wolbang, G. Prattes, H. Eichelberger, G. Stangl, M. Parrot and K. Schwingenschuh, Reception conditions of low

50 frequency (LF) transmitter signals onboard DEMETER microsatellite, Physics and Chemistry of the Earth, 102, 70–79, 2017.

Brown, L.W., The galactic radio spectrum between 130 kHz and 2600 kHz, Astrophys. J., 359–370, 1973.

Burch, J.L., IMAGE mission overview, Space Sci. Rev., 91, 1–14,

55 2000.

Carpenter, D.L., Bell, T.F., Inan, U.S., Benson, R.F., Sonwalkar, V.S., Reinisch, B.W., and D. L. Gallagher, Z-mode sounding within propagation "cavities" and other inner magnetospheric regions by the RPI instrument on the IMAGE satellite, J. Geophys.

60 Res., 108, A12, 2003.

Darrouzet, F., Gallagher, D. L., André, N., Carpenter, D. L., Dandouras, I., Décréau, P. M. E., De Keyser, J., Denton, R. E., Foster, J. C., Goldstein, J., Moldwin, M. B., Reinisch, B. W., Sandel, B. R., and J. Tu, Plasmaspheric Density Structures and Dynamics:

65 Properties Observed by the CLUSTER and IMAGE Missions, Space Sci. Rev., 145, 55–106, 2009.

Décréau, P. M. E., Ducoin, C., Le Rouzic, G., Randriamboarison, O., Rauch, J.-L., Trotignon, J.-G., Vallières, X., Canu, P., Darrouzet, F., Gough, M. P., Buckley, A. M., and T.D. Carozzi, Ob-

70 servation of continuum radiations from the Cluster fleet: first results from direction finding, Ann. Geophys., 22, 2607-2624, 2004.

Décréau, P. M. E., Fergeau, P., Krasnoselskikh, V., Le Guirriec, E., Lévêque, M., Martin, Ph., Randriamboarison, O., Rauch, J. L.,

75 Senée, F. X., Séran, H. C., Trotignon, J. G., Canu, P., Cornilleau, N., de Féraudy, H., Alleyne, H., Yearby, K., Mögensen, P. B., Gustafsson, G., André, M., Gurnett, D. C., Darrouzet, F., Lemaire, J., Harvey, C. C., Travnicek, P., and Whisper experimenters: Early results from the Whisper instrument on Cluster:

80 an overview, Ann. Geophys., 19, 1241-1258, 2001.

El–Lemdani Mazouz, F., J. L. Rauch, P. M. E. Décréau, J. G. Trotignon, X. Vallières, F. Darrouzet, P. Canu, and X. Suraud, Wave emissions at half electron gyroharmonics in the equato-

rial plasmasphere region: CLUSTER observations and statistics, Adv. Space Res., 43, 253-264, 2009.

Frankel, M.S., LF radio noise from the earth's magnetosphere, Radio Sci., 8, 991-1005, 1973.

Green, J. L., and S. A. Boardsen, Kilometric continuum radiation, Radio Sci. Bull., 318, 34- 41, 2006.

Green, J. L., S. Boardsen, S. F. Fung, H. Matsumoto, K. Hashimoto, R. R. Anderson, B. R. Sandel, and B. W. Reinisch, Association of kilometric continuum radiation with plasmaspheric structures, J. Geophys. Res., 109, A03203, 2004.

Grimald, S., El-Lemdani Mazouz, F., Foullon, C., Décréau, P. M. E., Boardsen, S. A., and X. Vallières, X.: Study of non-thermal continuum patches: wave propagation and plasmapause study, J. Geophys. Res., 116, A07219, 2011.

Grimald, S., Décréau, P. M. E., Canu, P., Rochel, A., and X. Vallières, Medium latitude sources of plasmaspheric non thermal continuum radiations observed close to harmonics of the electron gyrofrequency, J. Geophys. Res., 113, A11217, 2008.

Gurnett, D. A., The Earth as a radio source: The nonthermal continuum, J. Geophys. Res., 80, 2751–2763, 1975.

Gurnett, D. A., and L. A. Frank, Continuum radiation associated with low-energy electrons in the outer radiation zone, J. Geophys. Res., 81, 3875–3885, 1976.

Gurnett, D. A., and R. A. Shaw, Electromagnetic radiation trapped in the magnetosphere above the plasma frequency, J. Geophys. Res., 78, 8136- 8148, 1973.

Gurnett, D. A., Shawhan, S.D., and R. R. Shaw, Auroral hiss, Z-mode radiation, and auroral kilometric radiation in the polar magnetosphere: DE 1 observations, J. Geophys. Res., 88, 329, 1983.

Gurnett, D. A., Calvert, W., Huff, R. L., Jones, D., and M. Siguira, The polarization of escaping terrestrial continuum radiation, J. Geophys. Res., 93, 12817–12825, 1988.

Hashimoto, K., J. L. Green, R. R. Anderson, and H. Matsumoto, Review of kilometric continuum, in Geospace Electromagnetic Waves and Radiation, Lect. Not. in Phys., Eds. J. W. LaBelle and R. A. Treumann, Springer, New York, 687, 37–54, 2006.

Hashimoto, K., W. Calvert, and H. Matsumoto, Kilometric continuum detected by GEOTAIL, J. Geophys. Res., 104, 28,645-28,656, 1999.

Jones, D., Source of terrestrial nonthermal radiation, Nature, 260, 686-689, 1976.

Jones, D., Mode-coupling of Z mode waves as a source of terrestrial kilometric and Jovian decametric radiations, Astron. & Astrophys., 55, 245–252, 1977.

Jones, D., Beaming of terrestrial myriametric radiation, Adv. Space Res., 1,373, 1981.

Jones, D., W. Calvert, D. A. Gurnett, and R. L. Huff, Observed beaming of terrestrial myriametric radiation, Nature, 328, 391, 1987.

Kuril'chik, V.N., M. Y. Boudjada, H. O. Rucker, and I. F. Kopaeva, Observations of Electromagnetic Emissions inside the Earth's Plasmasphere from the INTERBALL-1 Satellite, Cosmic Res., 45, 455–460, 2007.

Kuril'chik, V.N, Boudjada, M.Y, and H.O. Rucker, The Observations of the Subauroral Nonthermal Radio Emission by AKR-X Receiver onboard of the INTERBALL Satellite, in Planetary Radio Emissions V, Eds. Rucker, H.O., Kaiser, M.L., and Leblanc, Y., Vienna: Austrian Academy of Sciences Press, 202–212, 2001.

Kurth, W. S., D. A. Gurnett, and R. R. Anderson, Escaping nonthermal continuum radiation, J. Geophys. Res., 86, 5519–5531, 1981.

Parrot M. and J.-J. Berthelier, AKR-like emissions observed at low altitude by the DEMETER satellite, J. Geophys. Res., 117, A10314, 2012.

Parrot, M., U. S. Inan, N. G. Lehtinen, and J. L. Pincon, Penetration of lightning MF signals to the upper ionosphere over VLF ground-based transmitters, J. Geophys. Res., 114, A12318, 2009.

Sandel, B.R., J. Goldstein, D.L. Gallagher and M. Spasojevic, Extreme ultraviolet imager observations of the structure and dynamics of the plasmasphere. Space Sci. Rev., 109, 25-46 2003.